RSC Advances

ROYAL SOCIETY OF CHEMISTRY

www.rsc.org/advances

Journal Name

ARTICLE

Improving supercapacitor performance of alkylated graphene nanosheets via partial fluorination on their alkyl chains†

Received 00th January 20xx,
Accepted 00th January 20xx

DOI: 10.1039/x0xx00000x

www.rsc.org/

Gang Zhao,[a,#] Fu-Gang Zhao,[b,#] Jianqing Sun,[a,#] Yang Lu,[a] Wei Wang,[a] Wei-Shi Li,[*,b] Qing-Yun Chen[*,a]

Redox-active graphene materials are highly desirable for the production of high performance supercapacitors. Following our previous work that found alkylated graphene nanosheets are a new kind of such materials, we report here the simple replacement of alkyl side chains with partially fluorinated alkyl chains further improve their capacitive electrode performance. In the work, one partially fluorinated graphene material (**pFAG**) was prepared by the reaction of KOH-pretreated graphene oxide with 2-perfluorohexylethyl bromide in the presence of a phase transfer catalyst. Compared with graphene material modified with octyl side chains (**AG**), **pFAG** possesses a larger amount of residue oxygen functionalities, which is favor to enable the material a redox-active nature and achieve a larger Faradic capacitance. Moreover, **pFAG** presented a special self-assembly behavior and formed continuous and large plate-like objects in solid state. Finally, a supercapacitor electrode was fabricated with **pFAG** and its performance was compared with the previous reported **AG**-based electrode in detail. It was found that the **pFAG** electrode has a much better capacitive performance than that based on **AG** (218.3 *vs*. 160.0 F g^{-1} at a scan rate of 100 mV s^{-1} by cyclic voltammetry, while 187.0 *vs*. 118.8 F g^{-1} at a current density of 3 A g^{-1} by galvanostatic charge/discharge method). When charge/discharge was carried out at 1 A g^{-1}, the specific capacitance of **pFAG**-based electrode reached 388.0 F g^{-1}, a value among the first class of the reported graphene-based electrodes. Furthermore, **pFAG** electrodes exhibited a good cycling stability. All these demonstrate graphene nanosheets modified with partial fluorinated alkyl chains would be a good way for achieving high performance redox-active electrode materials.

Introduction

As one of energy storage and supply devices, supercapacitors have advantages in terms of high energy capacity, high power density, and quick charge and discharge process, and thus provide one of promising solutions to increasing demands from the fields of portable electronics and electric vehicles.[1] Among numerous electrode materials developed for supercapacitors so far, graphene has attracted particular attention due to its striking large specific surface area (SSA, 2630 m^2 g^{-1} in theory) and outstanding electrical conductivity.[2] In the early era, the so-prepared devices mostly operated with electrochemical double-layer (EDL) mechanism since their electrodes were based on redox inactive graphene nanosheets only.[3] However, their capacitances were mostly in the range of 100–280 F g^{-1}, far from real demands.[2] For increasing energy storage capacity, the later works hybridized graphene materials with other redox-active components, such as polyanilines,[4] RuO_2,[5] or TiO_2,[6] etc. for supercapacitor electrodes. By this strategy, devices with a capacitance over 1000 F g^{-1} have been successfully achieved. However, in the most cases, devices were suffering from poor cycling stability and complicity in device fabrication. More recently, it was proposed to develop redox-active graphene materials by integration of certain redox-active moieties into carbon skeleton for achieving additional Faradic capacitance besides EDL mechanism and simplifying fabrication procedure. Thus, the decorations with heteroatoms, such as N[7] and B,[8] and the reservation of certain oxygen-containing functionalities on the surface of carbon nanosheets by special acid-assisted ultra-rapid thermal processing on graphene oxide (**GO**)[9] were reported. Recently, we found simply alkylation of KOH-pretreated **GO** has the similar effect: partial oxygen-containing functionalities were successfully survived during the treatment and thus endowed the material Faradic capacitance.[10] Of interest, the supercapacitor performance of so-produced graphene materials showed a special alkyl length-dependent effect, with 242.2 F g^{-1} for the butyl-modified, while 160 F g^{-1} for the octyl case. In this contribution, we report an

[a] *Key Laboratory of Organofluorine Chemistry, Shanghai Institute of Organic Chemistry, Chinese Academy of Sciences, 345 Lingling Road, Shanghai 200032, China. E-mail: chenqy@sioc.ac.cn*
[b] *Key Laboratory of Synthetic and Self-Assembly Chemistry for Functional organic Molecules, Shanghai Institute of Organic Chemistry, Chinese Academy of Sciences, 345 Lingling Road, Shanghai 200032, China. E-mail: liws@mail.sioc.ac.cn.*
[#] These authors contributed to this work equally.
† Electronic Supplementary Information (ESI) available: Raman spectrum of **pFAG** N_2 absorption and desorption isotherms of **pFAG**, and CV curves of **pFAG** electrode and Ni foam at a scan rate of 20 mV s^{-1}. See DOI: 10.1039/x0xx00000x

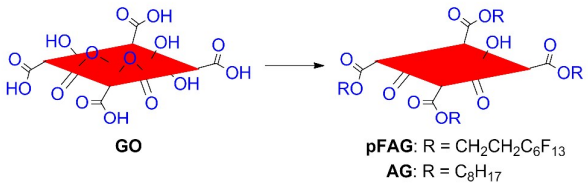

Scheme 1 Preparation of alkylated and partially fluorinated alkylated graphene materials. Reagents and conditions: 1) KOH, sonication; 2) 2-perfluorohexylethyl bromide for **pFAG**, while octyl bromide for **AG**, $(C_8H_{17})_4NBr$, reflux.

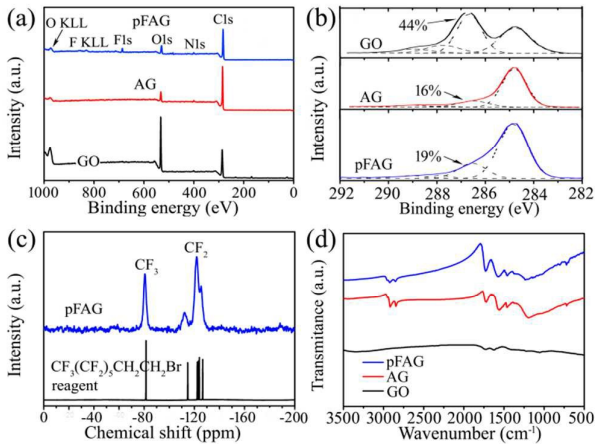

Fig. 1 (a) XPS spectra and (b) their enlarged region around C 1s peaks of **GO**, **AG**, and **pFAG**. (c) Solid-state ^{19}F NMR spectra of **pFAG** and perfluorohexylethyl bromide. (d) FT-IR spectra of **GO**, **AG**, and **pFAG**.

unexpected finding: the replacement of octyl side chains with partially fluorinated octyl chains vastly improved material supercapacitor performance with a specific capacitance up to 388.0 F g^{-1} at 1 A g^{-1}, overbidding that of the butyl case in the previous work.[10]

Results and discussion

The preparation of partially fluorinated alkylated graphene nanosheets (**pFAG**) followed the same method as that of the alkylated graphene materials (Scheme 1).[10] Namely, **GO** was firstly treated with KOH to remove instable oxygen-containing functionalities on nanosheet surface, and meanwhile to convert the surviving edge carboxylic acid units into potassium carboxylate functionality. After esterification with perfluorohexylethyl bromide in the presence of $(C_8H_{17})_4NBr$ as a phase transfer catalyst, **pFAG** was produced. For the purpose of comparison, graphene material modified with octyl side chains in our previous work[10] (the name of **AG** is used here to replace the previous one, **C_8rGO**) were used as reference and its relative data are included again in this paper.

The successful integration of partially fluorinated alkyl chains into the carbon nanosheets in **pFAG** was confirmed by elemental analysis, X-ray photoelectron spectroscopy (XPS), and particularly solid-state ^{19}F NMR. By means of a typical oxygen flask combustion method, **pFAG** was found to have an F content of 4.4%. In XPS, **pFAG** displayed a typical F 1s core level peak around 689 eV,[11a] which did not appear in the spectra of **AG** and **GO** (Fig. 1a). More detail information comes from its solid-state ^{19}F NMR, in which four typical peaks around -80.5, -112.2, -121.8 and -125.4 ppm were observed (Fig. 1c). Since these peaks were similar to those in the spectrum of 2-perfluorohexylethyl bromide, their assignment can be deduced as follows: the first peak from CF_3 moiety, while the latter three from CF_2 units. Besides, Fourier transform infrared spectroscopy (FT-IR) also consolidated the successful attachment of partially fluorinated alkyl chains to carbon nanosheets by the presence of CH_2 characteristic vibration peaks at 2920 and 2850 cm^{-1} (Fig. 1d).

The reduction of **GO** nanosheets during fluoroalkylation was further confirmed by Raman spectroscopy. In Raman spectroscopy, chemically derived graphene usually has two characteristic stretching bands around 1590 (G band) and 1350 cm^{-1} (D band). The former originates from the perfect graphene structure, while the latter from disordered structure having defects of sp^3-hybridized carbons. Their area-intensity ratio (I_D/I_G) reflects the amount of disorder domains in graphitic structures. In our work, the I_D/I_G of **pFAG** was estimated to be 1.72 (Fig. S1†), which is smaller than that of **GO** (1.81).[10] This is similar to the observation in our previous work, in which **AG** also showed a decreased I_D/I_G value (1.48) compared to **GO**. However, based on the assumption that **GO** has not been reduced during the reaction, this I_D/I_G would become larger because of the increasing content of sp^3 carbon by alkyl chains. The contrary observation suggests **GO** was reduced and graphene structures were restored during the fluoroalkylation reaction. This is not strange since Zhang *et al*. already demonstrated that **GO** undergoes reduction by treatment of KOH or NaOH in aqueous media.[11b]

Furthermore, the above elemental analysis, XPS and IR characterizations also suggest **pFAG** possesses certain amount of oxygen-containing functionalities. For example, besides the above 4.4% F content, elemental analysis revealed C, H, and N contents in **pFAG** to be 68.6%, 7.4%, and 1.4%, respectively, thus giving an O content of 18.2%. This value is far smaller that of **GO** (43.9%), but slightly larger than that of **AG** (15.6%).[10] In XPS spectrum of **pFAG**, the appearance of O 1s core level signal at 533 eV also confirms the presence of certain oxygen functionalities, although its intensity greatly decreased as compared to that of **GO** (Fig. 1a). Furthermore, the deconvolution of the C 1s peak yielded four components centred at 284.5, 285.6, 288.6 and 289.6 eV, associating with C–C/C=C, C–O, C=O, and COOH moieties, respectively (Fig. 1b).[12] For C-O component of **pFAG**, the population was estimated to be 19%. The value is again smaller than that of GO (44%), but slightly larger than that of **AG** (16%).[10] In IR spectroscopy, the vibration peaks at 1729 and 1223 cm^{-1} originating from ester and C-O functionalities respectively, appeared in both spectra of **pFAG** and **AG** (Fig. 1d). As aforementioned, these remained oxygen-containing moieties would play an important role that enable graphene materials

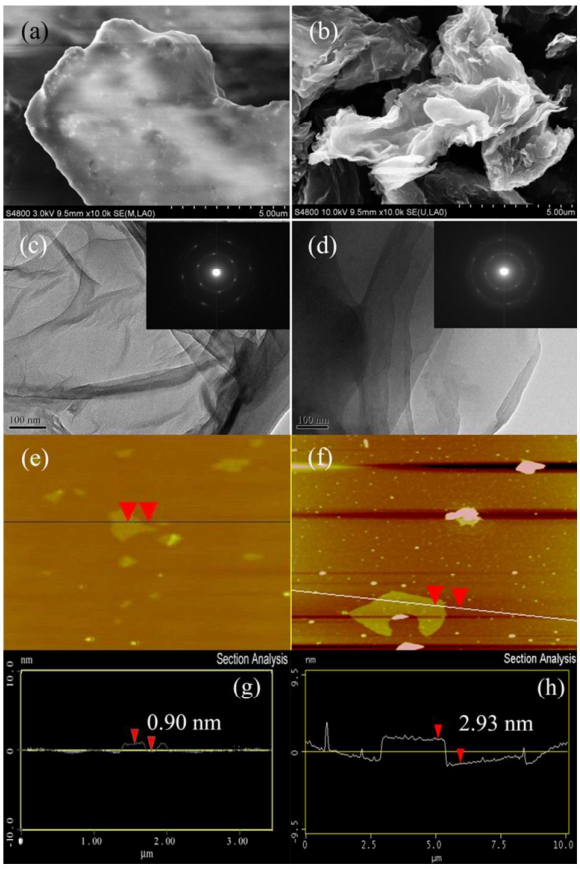

Fig. 2 (a, b) SEM, (c, d) TEM, (e, f) AFM images and (g, h) AFM height profiles of (a, c, e, g) **pFAG** and (b, d, f, h) **AG**. Insets of (c, d) are their SAED patterns.

redox active.[9, 10] Therefore, the higher residue oxygen content for **pFAG** would improve its redox activity and endow the material a larger Faradic capacitance.

The morphology and nanosheet structure of **pFAG** were investigated by means of scanning electron microscopy (SEM), transmission electron microscopy (TEM), and atomic force microscopy (AFM). As shown in Fig. 2a, SEM observation was performed on **pFAG** solid samples and revealed a continuous and large plate-like morphology. Such appearance is quite different from that of **AG**, which looks like the pile of nano-plates (Fig. 2b).[10] Since fluoroalkyl chains are more hydrophobic than alkyl chains and possess a special fluorophilic effect, the formation of such a structure may be ascribed to special communication among fluoroalkyl side chains and inter-sheet π-π stacking interactions. In TEM, transparent silk-like sheets were visualized for both **pFAG** and **AG** (Fig. 2c and 2d). However, careful observation will find **pFAG** nanosheets appeared to be much softer than those of **AG** and full of wrinkles. Moreover, a well-defined six symmetrical spot pattern was identified in the normal incident selected area electron diffraction (SAED) on **pFAG** nanosheets (Fig. 2c, inset). In comparison, two clear diffraction rings together with faint six symmetrical diffraction spots appeared in the SAED of **AG** nanosheets.[10] These observations suggest that **pFAG** nanosheets may have a monolayer graphene characteristic, whereas **AG** nanosheets are few-layer graphene. And, this deduction was further supported by atomic force microscopy (AFM), in which the sheet thickness was estimated to be 0.9 nm of **pFAG**, while 2.93 nm for **AG** (Fig. 2e–2h).

Specific surface area (SSA) is one of important factors that determine potential usage for a material for supercapacitor electrode application. High capacitor performance requires the material have a large specific surface area. In this work, material SSA values were measured by means of two methods, an usual Brunauer-Emmett-Teller (BET) way and a dye-absorption way.[10, 13] BET method was applied on solid samples and based on nitrogen absorption and desorption isotherms. As shown in Fig. S2†, **pFAG** materials displayed an ideal type II nitrogen absorption isotherm, which can be analysed by BET theory to know its SSA datum (13.18 $m^2 g^{-1}$). The so small value may be ascribed to severe aggregation in solid state for **pFAG** sample, coinciding with the aforementioned SEM observations. In comparison, the BET SSA data of **AG** and **GO** samples measured under the same conditions in our previous work are only 11.22 and 4.48 $m^2 g^{-1}$, respectively.[10] Thereby, **pFAG** has a larger SSA value than both **AG** and **GO**, implying a much more promising usage for supercapacitor electrode. However, SSA data measured by dye absorption method were quite different from the above BET results. This method was carried out in water dispersion and used methylene blue dye (MB) as a probe. In such conditions, all dispersible carbon nanosheets would stay in segregate stage and open all possibly active surfaces for dye absorption. By this method, **pFAG** was reported to have a SSA of 1091 $m^2 g^{-1}$, greatly larger than the above BET value. However, this value is very close to that of **AG** (1110 $m^2 g^{-1}$ reported previously[10]) and not consistent with its monolayer structure suggested by TEM and AFM. Ideally, **pFAG** should have a value close to the theoretical SSA of graphene (2630 $m^2 g^{-1}$) and would be much larger than few-layer structured **AG**. Although the real reason for this small SSA datum obtained is unknown at present, we deduce that partially fluorinated alkyl side chains may impede dye absorption owing to their super-hydrophobic nature. In our previous work, similar phenomena were observed: the longer alkyl side chains, the thinner layer structure observed by AFM, but the smaller SSA value obtained by dye absorption method.[10]

In addition to specific surface area, electrical conductivity is another important factor for electrode materials. Fortunately, **pFAG** was found to be electrically conductive and have a conductivity of 47.5 S m^{-1}. Such a conductivity is larger than that of **AG** (25.1 S m^{-1}) reported previously.[10] When considering that fluoroalkyl chains are generally more electrically insulating than alkyl chains, one may reasonably deduce that the formation of continuous and large plate-like structure in solid state, as revealed by SEM (Fig. 2a), would help **pFAG** to achieve a large electrical conductivity.

The supercapacitor performance of **pFAG** was investigated by cyclic voltammetry (CV) and galvanostatic charge/discharge

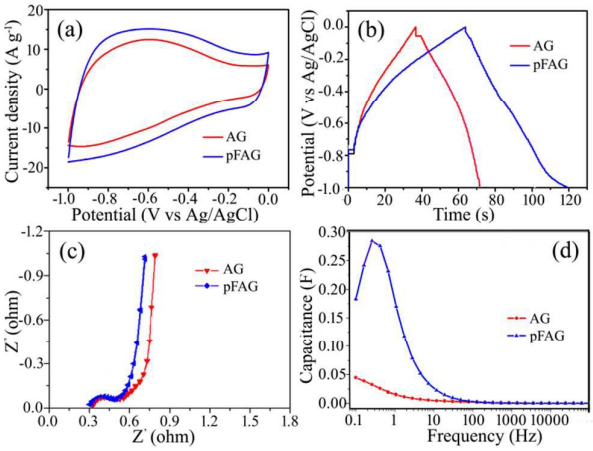

Fig. 3 (a) CV at a scan rate of 100 mV s^{-1}, (b) CD curves at a current density of 3 A g^{-1}, (c) Nyquist plots, and (d) the specific capacitance as a function of the frequency for the electrodes based on **pFAG** and **AG**.

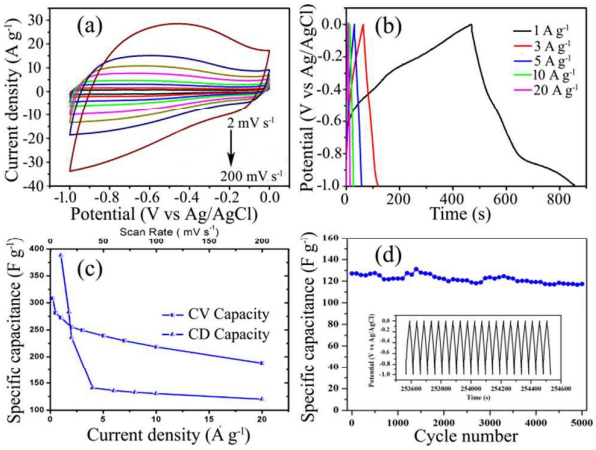

Fig. 4 (a) CV curves at various scanning rate, (b) CD profiles at different current densities, (c) the dependences of specific capacitance on CV scan rate and CD current density shown in (a) and (b), respectively, and (d) cycling stability at a current density of 5 A g^{-1} for **pFAG** electrode. The curve for the last 20 charge–discharge cycling is shown as inset.

(CD) analysis on a **pFAG** based electrode in 6 M aqueous KOH solution. This electrode was prepared by painting slurry of **pFAG**, polytetrafluoroethylene (PTFE) and carbon black in a weight ratio of 85: 15: 5 to a plate of Ni foam. Here, the contribution of Ni foam in electrochemical measurements was negligible as compared to the prepared electrode (Fig. S3†). Fig. 3a displays one typical CV curve of **pFAG** electrode, which looks like a rectangle loop superimposed with one pair of broad Faradic peaks in the range of -0.3 to -1.0 V and resembles that of **AG**. This indicates the coexistence of EDL and Faradic pseudo capacitances for both **pFAG** and **AG** electrodes. It was reported that hydroxyl and carbonyl in carbon materials can provide certain redox reactions for pseudocapacitance.[2, 9, 10] Since both **pFAG** and **AG** possess certain amount of oxygen-containing functionalities, the observation of Faradic pseudo capacitive behaviour is not surprising. With these CV curves, the specific capacitances for both **pFAG** and **AG** electrodes were estimated to be 218.3 and 160.0 F g^{-1} at a scan rate of 100 mV s^{-1}, respectively. For reference, the electrode based on their starting material, **GO**, exhibited a specific capacitance of 122.7 F g^{-1}.[10] Obviously, **pFAG** has a better supercapacitor performance than **AG** and **GO**. This finding was further consolidated by CD measurements (Fig. 3b). The charge and discharge curves at a current density of 3 A g^{-1} for **pFAG** electrode provided a specific capacitance of 187.0 F g^{-1}. While under the same conditions, the **AG** electrode gave a CD curve having a specific capacitance of 118.8 F g^{-1}.[10]

The different supercapacitor performance between **pFAG** and **AG** electrodes can be firstly understood by the electrochemical impedance analysis (Fig. 3c and 3d). Compared with that based on **AG**, **pFAG** electrode displayed an almost vertical line at low frequency portion, a much shorter and less gradually sloping line at intermediate frequency portion, and a much smaller semicircle at high frequency portion in its Nyquist plot, suggesting a lower diffusion and charge-transfer resistance. Secondly, the higher content of residue oxygen-containing functionalities of **pFAG** than **AG** nanosheets, as confirmed by aforementioned elemental analysis and XPS, would be another factor for its better capacitive performance. Moreover, the different electronic effect of alkyl and fluoroalkyl chains would be the third factor. It is well known that alkyl side chains are electron-donating, which increase the electron density of modified moieties and make them hard to reduce. In contrast, fluoroalkyl chains are electron-withdrawing, which reduce the electron density of modified moieties and make them redox-active in the negative CV scanning region. Such phenomena are well documented in the field of organic semiconductors that the modification of π-functional molecules and polymers with fluoroalkyl side chains turns their charge-transportation nature from p-type to n-type.[14] Finally, as revealed by SEM, a much different self-assembly behaviour presented by **pFAG** as compared with **AG** maybe also contribute its better supercapacitor performance. Although many possibilities are shown above, the real accounts for better capacitive performance of **pFAG** than **AG** are not yet clear and worthy of further study.

Since **pFAG** is a good supercapacitor electrode material, more detail experiments were carried out to further understand its electrochemical performance. Fig. 4a displays its CV curves at different scanning rate. With the decrease in scan rate, the specific capacitance increased gradually and reached 308.1 F g^{-1} at a scan rate of 2 mV s^{-1} (Fig. 4c). When the scan rate was raised to 200 mV s^{-1}, the specific capacitance of the electrode still has a value of 188.2 F g^{-1}. This result implies that **pFAG** electrode not only processes a large specific capacitance but also presents a significant competitive rate capability as well. From its CD experiments with different current density up to 20 A g^{-1} (Fig. 4b), **pFAG** electrode was estimated to have a specific capacitance of 388.0 F g^{-1} at a

current density of 1 A g^{-1} and 120.1 F g^{-1} at 20 A g^{-1} (Fig. 4c). These data are among the first-top level for graphene-based electrodes without combination with other redox-active components.[2] Furthermore, the cycling experiment showed a good cycling stability for **pFAG** electrode, which capacitance remained 84.8 % of the initial value after 5000 cycles at a current density of 5 A g^{-1} (Fig. 4d).

Conclusions

We have demonstrated here graphene nanosheets modified with partially fluorinated alkyl side chains (**pFAG**) have a better supercapacitor performance than those modified with alkyl side chains (**AG**). Although their preparation methods were the same, **pFAG** possessed a little larger amount of residue oxygen-containing moieties than **AG**. The different nature of partially fluorinated alkyl chains from that of alkyl ones endows **pFAG** a different self-assembly behaviour. Furthermore, the **pFAG** electrode showed a much lower internal resistance than that based on **AG**. All these factors together with the possibly different electron-withdrawing effect other than electron-donating effect on the modified moieties afford **pFAG** a much better electrochemically capacitive performance than **AG**. Its specific capacitance reached a value of 388.0 F g^{-1} at a current density of 1 A g^{-1}, which is among the first class in the reported graphene-based electrodes.

Experimental Section

Materials and general methods

Unless indicated, all commercial chemicals were used as received. Graphene oxide (**GO**) was prepared in the previous work[10], which followed a modified Hummers method.[15] Elemental analysis on C, H, and N contents was performed on an Elementar Vario EL III elemental analyzer. The content of F was measured by means of a typical oxygen flask combustion method. Solid state ^{19}F NMR spectra were recorded on a Bruker Avanced^{III} 376 MHz spectrometer. X-ray photoelectron spectra (XPS) were measured on a PHI-5000 VersaProbe spectrometer under 10^{-7} Pa using monochromatic Al K_α X-ray source operating at 100 W. Fourier transform infrared (FT-IR) spectra were measured on a Nicolet AVATAR-360 Fourier transform infrared spectrophotometer. Raman spectroscopy was carried out on a Renishaw via Reflex micro-Raman spectrometer using a 100-fold objective lens and a crystal laser excitation of 514.5 nm. Scanning electron microscopy was recorded on a Hitachi S-4800 field emission scanning electron microscope (FE SEM) operating at 3 kV. Transmission electron microscopy (TEM) and selected area electron diffraction (SAED) were performed on a JEOL JEM-200CX microscope operating at 120 kV. Atomic force microscopy (AFM) was carried out under ambient conditions on a Veeco Instruments Nanoscope IIIa Multimode apparatus operating in a non-contact mode with a silicon tip and cantilever operating at a frequency of 325 kHz and a scanning speed of 1.5 Hz. Samples were prepared by placing a drop of very dilute DMF dispersion on a mica substrate and dried in vacuum at room temperature.

Synthesis of pFAG.

GO (200 mg) was added to a KOH aqueous solution (0.1 M, 100 mL), and followed by ultrasonication for 2 h. Then, the pH of the mixture was adjusted to be 8–9 with dilute hydrochloric acid. After 2-perflorohexyl ethyl bromide (1.2 g, 2.81 mmol) and tetraoctylammonium bromide (50 mg, 0.09 mmol) were added, the reaction mixture was stirred at 100 °C for 2 h, and then cooled to room temperature and filtered by the nylon membrane with a pore size of 0.45 μm. The filtrate cake was subsequently washed with water and methanol, and dried under vacuum, giving the final product of **pFAG**. Elemental analysis found (%): C 68.6, H 7.4, N 1.4, F 4.4.

Specific surface area measurement

Similar to our previous work,[10] two methods were used for specific surface area measurement. One method followed Braunauer-Emmett-Teller (BET) theory. In this method, a Micromeritics accelerated surface area porosimetry (ASAP 2020, USA) autoadsorption analyzer was used to obtain N_2 adsorption and desorption isotherms at 77 K. Prior to the gas sorption measurements, all the samples were outgassed in a vacuum at 120 °C for 24 h. Finally, the N_2 absorption isotherms in the range of relative pressure (P/P_0) from 0.1 to 0.3 were used for multipoint BET calculations for specific area surface.

Another method adopted dye absorption way in dispersions.[13] Here, methylene blue (MB) was used as a dye probe since its molecules tend to absorb onto the entire available graphite surface in water medium. In a typical experiment, the sample (62 mg) were dispersed in a MB aqueous solution (2 g L^{-1}, 50 mL) and stirred for 3 h, followed by standing overnight. Afterward, the upper clear layer was sampled and its concentration was detected via UV-vis absorption spectroscopy using a wavelength of 298 nm. Since each mg of MB can absorbed on to 2.54 m^2 surface,[13] the specific surface area SSA (m^2 g^{-1}) of the sample can be calculated by the following equation:

$$SSA = \frac{(C_0 - C)V}{W} \times 2.54 \times 10^3$$

where *SSA* (m^2 g^{-1}), *W* (g), C_0 (g mL^{-1}), *C* (g mL^{-1}) and *V* (mL) are the specific surface area, sample quality, the average cross-sectional area of MB molecule, original and concentration, and solution volume, respectively.

Fabrication of pFAG electrode and electrochemical measurements

The studied **pFAG** electrode was prepared by mixing **pFAG** with carbon black and polytetrafluoroethylene (PTFE) in ethanol with a weight ratio of 85: 15: 5 to form slurry. Then, the slurry was painted onto one side surface of nickel foam with an area of 1 cm^2. Afterward, the electrode was folded and pressed under a pressure of 7.5 MPa. The mass loading of **pFAG** was 5.86 mg.

Electrochemical measurements followed the same methods reported in our previous work.[10] The experiments were performed on a Princeton PARSTAT 2273 electrochemical station and a Land CT2001A instrument with a three-electrode system composed of prepared **pFAG** electrode, a Pt plate electrode and an Ag/AgCl electrode as working, counter and reference electrode, respectively. A KOH solution (6 M) was used as electrolyte and the measurement was carried out at room temperature.

The electrode specific capacitance was calculated from the cyclic voltammetry (CV) curves according to the following formula:

$$C = \frac{1}{2m\Delta V}\int_{V_{initial}}^{V_{final}} \frac{I}{dV/dt}\,dV$$

where C (F g^{-1}) is the specific capacitance, m (g) is the mass of the active materials in the electrodes, ΔV (V) is the potential window, $V_{initial}$ (V) and V_{final} (V) are the starting and end potential in one cycle, I (A) is the instantaneous current at a given potential, and dV/dt is the potential scanning rate.

The discharge specific capacitance is calculated from the discharge curves using the following formula:

$$C = \frac{I\,\Delta t}{\Delta V m}$$

where I (A), Δt (s), m (g), and ΔV (V) are the discharge current, discharge time consumed in the potential range of ΔV, mass of the active materials, and the potential windows, respectively.

Acknowledgements

This work was supported by Natural Science Foundation of China (21032006, 21074147, and 21504080), and the 973 Program of China (2012CBA01200). We thank Professor Jinbo Hu of Shanghai Institute of Organic Chemistry for the electrochemical test equipment support.

Notes and references

1 P. J. Hall, M. Mirzaeian, S. I. Fletcher, F. B. Sillars, A. J. R. Rennie, G. O. Shitta-Bey, G. Wilson, A. Cruden and R. Carter. *Energy Environ. Sci.*, 2010, **3**, 1238.

2 (a) Y. Sun, Q. Wu and G. Shi, *Energy Environ. Sci.*, 2011, **4**, 1113. (b) Y. Zhai, Y. Dou, D. Zhao, P. F. Fulvio, R. T. Mayes and S. Dai, *Adv. Mater.*, 2011, **23**, 4828. (c) G. Wang, L. Zhang and J. Zhang, *Chem. Soc. Rev.*, 2012, **41**, 797. (d) L. Hao, X. Li and L. Zhi, *Adv. Mater.*, 2013, **25**, 38994. (e) R. R. Salunkhe, Y.-H. Lee, K.-H. Chang, J.-M. Li, P. Simon, J. Tang, N. L. Torad, C.-C. Hu and Y. Yamauchi, *Chem. Eur. J.*, 2014, **20**, 13838.

3 (a) M. D. Stoller, S. Park, Y. Zhu, J. An and R. S. Ruoff, *Nano Lett.*, 2008, **8**, 3498. (b) Y. Zhu, S. Murali, M. D. Stoller, K. J. Ganesh, W. Cai, P. J. Ferreira, A. Pirkle, R. M. Wallace, K. A. Cychosz, M. Thommes, D. Su, E. A. Stach and R S. Ruoff, *Science*, 2011, **332**, 1537.

4 L. Lai, H. Yang, L. Wang, B. K. Teh, J. Zhong, H. Chou, L. Chen, W. Chen, Z. Shen, R. S. Ruoff and J. Lin, *ACS Nano*, 2012, **6**, 5941.

5 Z.-S. Wu, D.-W. Wang, W. Ren, J. Zhao, G. Zhou, F. Li and H.-M. Cheng, *Adv. Funct. Mater.*, 2010, **20**, 3595.

6 X. Sun, M. Xie, G. Wang, H. Sun, A. S. Cavanagh, J. J. Travis, S. M. George and J. Lian. *J. Electrochem. Soc.*, 2012, **159**, 364.

7 L. L. Zhang, X. Zhao, H. Ji, M. D. Stoller, L. Lai, S. Murali, S. Mcdonnell, B. Cleveger, R. M. Wallace and R. S. Ruoff. *Energy Environ. Sci*. 2012, **5** 9618.

8 J. Han, L. L. Zhang, S. Lee, J. Oh, K. Lee, J. R. Potts, J. Ji, X. Zhao, R. S. Ruoff and S. Park, *ACS Nano*, 2013, **7**, 19.

9 Y. Fang, B. Luo, Y. Jia, X. Li , B. Wang, Q. Song, F. Kang and L. Zhi, *Adv. Mater.*, 2012, **24**, 6348.

10 G. Zhao, F-G. Zhao, J. Sun, Y. Lu, W. Wang, W-S. Li and Q-Y. Chen. *Carbon*, 2015, **94**, 114.

11 (a) F.-G. Zhao, G. Zhao, X.-H. Liu, C.-W. Ge, J.-T. Wang, B.-L. Li, Q.-G. Wang, W.-S. Li and Q.-Y. Chen, *J. Mater. Chem. A*, 2014, **2**, 8782. (b) X. Fan, W. Peng, Y. Li, X, Li, S. Wang, G Zhang and F. Zhang. *Adv. Mater.*2008, **20**, 4490.

12 (a) W. Chen, L. Yan and P. R. Bangal, *Carbon*, 2010, **48**, 1146. (b) F.-G. Zhao and W.-S. Li, *J. Mater. Chem.*, 2012, **22**, 3082.

13 M. l. J. McAllister, J.-L. Li, D. H. Adamson, H. C. Schniepp, A. A. Abdala, J. Liu, M. Herrera-Alonso, D. L. Milius, R. Car, R. K. Prud'homme and I. A. Aksay, *Chem. Mater.*, 2007, **19**, 4396.

14 (a) C. Wang, H. Dong, W. Hu, Y. Liu and D. Zhu, *Chem. Rev.* 2012, **112**, 2208. (b) Y. Zhao, Y. Guo and Y.Liu, *Adv. Mater.* 2013, **25**, 5372.

15 W. Hummers and R. Offman, *J. Am. Chem. Soc.*, 1958, **80**, 1339.